Quantitative measurement for the microstructural parameters of nano-precipitates in Al-Mg-Si-Cu alloys

*Title Page

Quantitative measurement for the microstructural parameters of nano-precipitates in Al-Mg-Si-Cu alloys

Kai Li[a,b,c], Hosni Idrissi[b,d], Gang Sha[e], Min Song[c,*], Jiangbo Lu[f], Hui Shi[b,g], Wanlin Wang[a], Simon P. Ringer[h,i], Yong Du[c], Dominique Schryvers[b]

[a]School of Metallurgy and Environment, Central South University, Changsha 410083, China

[b]Electron Microscopy for Materials Science (EMAT), University of Antwerp, Antwerp B-2020, Belgium

[c]State Key Laboratory of Powder Metallurgy, Central South University, Changsha 410083, China

[d]Institute of Mechanics, Université Catholique de Louvain, Louvain-la-Neuve 1348, Belgium

[e]Gleiter Institute of Nano-science, Nanjing University of Science and Technology, Nanjing 210094, China

[f]Electronic Materials Research Laboratory, Key Laboratory of the Ministry of Education and International Center for Dielectric Research, Xi'an Jiaotong University, Xi'an 710049, P. R. China

[g]ArcelorMittal Global R&D Gent, Pres. J.F. Kennedylaan 3 Zelzate, Gent B-9060, Belgium

[h]Australian Institute for Nanoscale Science and Technology, The University of Sydney, NSW, 2006, Australia

[i]School of Aerospace, Mechanical and Mechatronic Engineering, The University of Sydney, NSW, 2006, Australia

Abstract

Size, number density and volume fraction of nano-precipitates are important microstructural parameters controlling the strengthening of materials. In this work an widely accessible, convenient, moderately time efficient method with acceptable accuracy and precision has been provided for measurement of volume fraction of nano-precipitates in crystalline materials. The method is based on the traditional but highly accurate technique of measuring foil thickness via

convergent beam electron diffraction. A new equation is proposed and verified with the aid of 3-dimensional atom probe (3DAP) analysis, to compensate for the additional error resulted from the hardly distinguishable contrast of too short incomplete precipitates cut by the foil surface. The method can be performed on a regular foil specimen with a modern LaB_6 or field-emission-gun transmission electron microscope. Precisions around ±16% have been obtained for precipitate volume fractions of needle-like β″/C and Q precipitates in an aged Al-Mg-Si-Cu alloy. The measured number density is close to that directly obtained using 3DAP analysis by a misfit of 4.5%, and the estimated precision for number density measurement is about ±11%. The limitations of the method are also discussed.

Keywords: Aluminum alloys; 3DAP; foil thickness; volume fraction; transmission electron microscopy

*Corresponding author: msong@csu.edu.cn

Research highlights

1. An widely accessible, convenient, moderately time efficient method with acceptable accuracy and precision has been provided for measurement of volume fraction of nano-precipitates in crystalline materials.

2. A new equation has been proposed and verified with the aid of 3-dimensional atom probe (3DAP) analysis, to reduce the errors of determined precipitate volume fractions due to too small invisible precipitates.

3. The method was proved to have precisions around ±16% for precipitate volume fraction and ±11% for precipitate number density, displaying an improvement over the existing approaches.

Abstract

Size, number density and volume fraction of nano-precipitates are important microstructural parameters controlling the strengthening of materials. In this work an widely accessible, convenient, moderately time efficient method with acceptable accuracy and precision has been provided for measurement of volume fraction of nano-precipitates in crystalline materials. The method is based on the traditional but highly accurate technique of measuring foil thickness via convergent beam electron diffraction. A new equation is proposed and verified with the aid of 3-dimensional atom probe (3DAP) analysis, to compensate for the additional error resulted from the hardly distinguishable contrast of too short incomplete precipitates cut by the foil surface. The method can be performed on a regular foil specimen with a modern LaB_6 or field-emission-gun transmission electron microscope. Precisions around ±16% have been obtained for precipitate volume fractions of needle-like β″/C and Q precipitates in an aged Al-Mg-Si-Cu alloy. The measured number density is close to that directly obtained using 3DAP analysis by a misfit of 4.5%, and the estimated precision for number density measurement is about ±11%. The limitations of the method are also discussed.

Keywords: Aluminum alloys; 3DAP; foil thickness; volume fraction; transmission electron microscopy

1. Introduction

Quantification of typical microstructures plays an important role in deep understanding of phase transformations in materials and provides clues to the mechanisms controlling the materials' properties. Recent progress in quantitative simulations of the microstructures and mechanical properties based on methods such as CALculation of PHAse Diagrams (CALPHAD) [1, 2], multi-phase field simulation method [3, 4] and yield strength modeling [5] further enhances this importance because all these methods need accurate experimental verifications concerning the microstructures. Among the many microstructural parameters, the combination of size and number density of particles drastically affects the hardness and strength of the materials. For example, an intra-granular microstructure with fine needle-like nano-precipitates occurring in a high number density can double or triple the strength of Al-Mg-Si(-Cu) alloys [6, 7].

Various methods have been established to quantify the many aspects of the microstructures such as texture, solute segregation, volume fraction (i.e. product of size and number density) of second phase particles, grain size and so on. For example, the recent progress in X-ray nano-tomography [8, 9] and serial-sectioning using SEM/FIB (scanning electron microscopy with focused ion beam) [10, 11] has made it possible to visualize different phases in 3D with varying sizes from several tens of microns down to several tens of nanometers. It is also possible to observe nano-objects (with at least one dimension below 10 nm) in 3D by quantitative electron tomography and thus to obtain their volume fraction [12-14]. However, a risk of beam damage exists due to the long exposure time (typically up to 46 min in total) required for the acquisition of serial images at a wide range of tilts. The risk and the sacrifice of time (including that of image interpretation) can be avoided if one is not interested in the very detailed shape of the particle/defect.

Generally, four methods have been applied to the measurement of size, number density and volume fraction of nano-precipitates in Al-Mg-Si(-Cu) alloys. By transmission electron microscopy (TEM), the number and size of nano-precipitates in a region can be measured from low-magnification bright field (BF) images and high-resolution TEM images. The volume of the observed region could be obtained by measuring the thickness of the region through electron energy-loss spectrometry (EELS) [15, 16] (Method 1) and multiplying it with the area of the region. The thickness can also be estimated

by counting the number of extinction fringes either at the edge of a wedge-shaped TEM foil (Method 2) or at an inclined grain boundary (Method 3) [17]. On the other hand, the precipitate size and relative volume fraction can be directly calculated from a small-angle X-ray scattering (SAXS) profile [18, 19] (Method 4).

However, there are several issues with regard to precisions and limitations of these four methods. The uncertainty of Method 1 for measuring the foil thickness can be as large as ±20% [20]. Although in recent years due to the accurate measurement of mean free path this uncertainty can be reduced to ±8% (e.g., for Al [21]), the error brought about is still not negligible. Moreover, not every TEM instrument is equipped with an expensive EELS apparatus. Method 2 requires an ideal wedge-shaped foil with a starting thickness of 0~0.5 ξ_g (ξ_g is the extinction distance of the chosen reflection) at the edge of the hole (see Fig. 1a for an example). Moreover, it can give only a rough estimate of foil thickness (except at the fringes) when the wedge angle is not constant. Method 3 can only obtain the approximate thickness of a region near a grain boundary, as shown in Fig.1b. The top and bottom ends of an inclined grain boundary in the foil are invisible, producing a large additional error. In method 4, the relative volume fraction also has an uncertainty as large as ±15%. Additionally, different types of concurrent precipitates [19] may have similar contributions to a SAXS profile.

In this work, efforts have been devoted to the establishment of a facile method for determination of size, number density and finally volume fraction of nano-precipitates with acceptable accuracy and precision. Such a method can be implemented on a modern TEM with LaB_6 filament or field emission gun (FEG) accessible to most microscopists (i.e., with no special additional apparatus equipped). Two techniques are used to establish such a method. The conventional technique of convergent beam electron diffraction (CBED) was reported to have a small uncertainty of ±3% [22] in determining TEM foil thickness. Moreover, its output does not contain the influence from the amorphous layer on the foil surface as is the case for EELS [20]. It is the most precise method for crystals that are thicker than ξ_g [23], and is thus used for measuring the volume fractions of the needle-like nano-precipitates in Al-Mg-Si(-Cu) alloys in this work. On the other hand, in recent years 3-dimensional atom probe (3DAP) can be applied for determining the number densities of nano-sized objects, such as atomic clusters, G.P.-zones and β″ precipitates [24], although acquiring the average sizes of such objects is believed to be less reliable due to the errors produced when selecting precipitates [25]. Therefore, in the present work the measurement of size, number density and volume fraction of nano-precipitates based

on CBED has been performed first, followed by verification using 3DAP. Limitations of the systematically established method are also discussed.

2. Materials and Methods

The Al-Mg-Si-Cu alloy studied in this work has a nominal composition of Al-1.0 wt.% Mg-1.1 wt.% Si- 0.65 wt.% Cu. The alloy was cast, solutionized at 550 ºC for 4 h and quenched, and then immediately aged at 175 ºC for different times. Details about casting, solution and ageing (at 175 ºC) heat treatments of the alloy as well as preparation of TEM foils have been described elsewhere [26, 27]. TEM observations were performed on a FEI G2 F20 microscope operated at 200 kV. The tip specimen for 3DAP analysis was prepared from a thin bar of 0.5 × 0.5 × 15 mm^3 cut from the alloy aged for 8 h, via the standard two-step electro-polishing procedures [28]. The tip was then examined in a LEAP 3000 SI instrument under a high vacuum of 10^{-12} Torr, at a specimen temperature of 20 K, a pulse repetition rate of 200 kHz and a pulse voltage fraction of 20%. The parameters used for analyzing the 3DAP results are separation distance (d) of 0.6 nm, surround distance of L = 0.5 nm for including solvent atoms and minimum cluster size (N_{min}) of 10 solutes. For identification of the boundary between the matrix and elongated precipitates like β", an isosurface at 5 at.% Mg [24, 29] has been defined, which reproduces a similar precipitate size to that measured by TEM. Similar methods for defining nano-precipitate surfaces have also been applied in other 3DAP investigations of Al alloys to obtain precipitate number densities [24, 25, 30, 31].

3. Results and discussion

The precipitation sequence of the alloy at 175 ºC has been identified as follows: super-saturated solid solution (SSSS) → G.P.-zones → β" + C (for 8 h) → Q + Si (for 30 d), according to our previous studies [26, 27]. Two typical intragrannular microstructures, i.e. the peak-aged (2#, for 8 h) and over-aged (1#, for 30 d), are selected for this work since they typically contain short and long needle-like nano-precipitates growing along $<001>_{Al}$ directions in high and low densities, respectively. According to high-resolution TEM (HRTEM) and high-resolution scanning transmission electron microscopy (HRSTEM) observations, the peak-aged microstructure is comprised of β" (~83%, identified in a previous work [26]) and C (~17%, identified as shown in Fig. S1 in the Supplement [32])

needle-like precipitates, while the over-aged microstructure contains coarser needle-like Q precipitates and micro-sized plate-like Si precipitates (identified in a previous work [27]). The microstructural parameters of Si precipitates are not measured in this work.

The measurement of size, number density and volume fraction of nano-precipitates is based on two important simplifications of the real microstructure: (a) uniform distribution of precipitates in intragranular regions; (b) equal size (and its dispersion) and number density of precipitates growing along the three axes of the f.c.c. α-Al matrix. Since as-cast Al alloys should all be homogenized and/or solutionized before ageing, the solute content in the intragranular region should generally be homogeneous. The imperfect precipitate free zone of about 100-200 nm in width is too small compared to the typical Al grain size of 10-100 μm and the observations in this work were all obtained from regions far away (> 10 μm) from the precipitate free zone. Therefore, simplification (a) can be regarded as reasonable while simplification (b) is acceptable since no deformation was performed on this alloy to cause possible preferential growth of the precipitates along one of the equivalent directions.

3.1 Quantification of Q precipitates in the over-aged microstructure based on CBED

The volume fraction (V_f) of the needle-like Q precipitates is the product of the average length (l), the average area of the transverse cross-section (A_{cs}) and the number density (n).

The length l has been measured in a series of TEM BF images taken along $[001]_{Al}$ as typically shown in Fig. 2a. About 300 precipitates were found growing along $[100]_{Al}$ and $[010]_{Al}$ in these images, and l has been measured as 103 ± 3.6 nm (mean value ± standard error). It should be stated that almost all of the needle-like nano-precipitates such as β", β', U1, U2, B', Q' and Q, with various cross-section shapes in aged Al-Mg-Si(-Cu) alloys, are fully coherent with the α-Al matrix along the growth directions. These phases have the same lattice parameter of 0.405 nm (3×0.405 nm for β') as that of α-Al along the growth directions, which is also the reason why a nano-precipitate tend to grow into needles, other than plates, cubes or tapered shapes and so on. Minor lattice misfits between precipitate/matrix exist along other directions perpendicular to the elongation direction, making the corresponding interfaces around the needle semicoherent [33-35]. The strain field provides effective impediment against dislocation movement and thus helps strengthening the material, meanwhile it displays noticeable contrast in even low-magnification TEM images and makes the nano-precipitates

easily distinguishable. For this reason the average length of nano-precipitates can be measured from 200 to 300 precipitates in low-magnification TEM images. The incomplete side-on nano-precipitates (e.g., those growing along $[100]_{Al}$ and $[010]_{Al}$ in Fig. 2a) located at the edges of the fields of view are not taken into account.

On the other hand, the average area of cross-section of the needles should only be measured in HRTEM images in order to avoid the overestimation caused by the strain field. Since acquisition of HRTEM image is more time consuming than that of low-magnification images, a smaller statistic of about 20 precipitates is used in this work. This leads to a larger relative error for the measurement of precipitate cross-section area than that for length. The measured area A_{cs} for Q precipitates is 18.9 ± 1.89 nm^2, as obtained from HRTEM images of 17 precipitates typically shown in the insets of Fig. 2a.

The number density of the Q precipitates has been measured from a thicker region (see Fig. 2b) in order to properly measure the thickness. Firstly, the number of precipitates contained in the region was estimated from those aligned along the viewing direction, e.g. $[001]_{Al}$ for the case shown in Fig. 2b. Viewing from the elongation direction of precipitates will guarantee the largest image contrast (partly due to the strain field) for these precipitates and reduce the probability for relatively fine nano-precipitates being unnoticed, although these precipitates are 2~4 nm wide and the atomic scattering factors for Mg and Si are very close to that for Al. Since the transverse cross sections of some Q precipitates can occasionally grow into squares or irregular shapes [27, 36], rather than rectangles as conventionally believed [7], all the end-on needle-like precipitates along $[001]_{Al}$ with different cross-section geometries were counted. Totally 282 precipitates were measured in Fig. 2b. The counted number of nano-precipitates growing along $[001]_{Al}$ are then extrapolated to all the nano-precipitates along $<001>_{Al}$ as explained above.

The region observed in Fig. 2b was then tilted slightly ($\Delta\alpha$ = 1.15˚, $\Delta\beta$ = 4.83˚) to obtain a two beam condition with a dark Kikuchi line crossing the 000_{Al} bright disk and a bright Kikuchi line crossing the 200_{Al} dark disk in the CBED pattern, as shown in Fig. 2c. The thickness of the region at this tilt can be calculated from the values of $2\theta_B$, $\Delta\theta_i$, $\Delta\theta_{i+1}$, $\Delta\theta_{i+2}$, $\Delta\theta_{i+3}$ and $\Delta\theta_{i+4}$ obtained from the pattern with *i-1* the integer number of extinction distances for reflection $g(200)_{Al}$ across the foil thickness. The S_i values are correspondingly calculated from the formula [20] of

$$S_i = \lambda\Delta\theta_i/(2\theta_B d^2) \qquad \text{Eq. (1)}$$

where λ represents the wave length of the electron beam and d is the corresponding d-spacing of

reflection $g(200)_{Al}$. With the appropriate i value, the relationship between S_i^2/n_k^2 and $1/n_k^2$ should follow the straight line formula of

$$S_i^2/n_k^2 = a \cdot 1/n_k^2 + b \ (n_k = i, i+1, i+2...) \quad \text{Eq. (2).}$$

The y interception b is equal to $1/t^2$ in which t is the thickness of the region across the incident beam direction. In the present case, an i value of 4 has been found to produce a straight line as shown in Fig. 2d with $b = 1.06181 \times 10^{-5}\ \text{nm}^{-2}$. As a consequence, the t value is calculated as $t_2 = 307$ nm. By considering the slight tilt of $\Delta\alpha = 1.15^\circ$, $\Delta\beta = 4.83^\circ$, the thickness t of the region in Fig. 2b is calculated as $t_1 = 309$ nm according to

$$t_1^2 / t_2^2 = (1+ \tan^2\alpha_1 + \tan^2\beta_1) / (1+ \tan^2\alpha_2 + \tan^2\beta_2) \quad \text{Eq. (3).}$$

It should be noted that this calculation is performed under the assumption of flat foil surface, i.e. the foil surfaces are normal to the incident electron beam at zero tilt. This assumption is reasonable according to the fact that the TEM foil is prepared by electro-polishing yielding a slight average slope of about 100 (thickness of the unpolished foil) μm / 1250 (radius of electro-polished area) μm, corresponding to an average inclination of 4.6º. This slight inclination should make the observed foil a little edge-shaped, however, as long as the position of thickness determination is located in the center of the field of view as in the case of this work, the determined thickness is geometrically the average thickness of the field of view. For this reason, the effect of slightly edge-shaped foil geometry can be ignored.

The extinction distance ξ_g of reflection $g(200)_{Al}$ is determined as 88.4 nm according to $a = -\xi_g^{-2}$. The theoretical ξ_g can be calculated from the equation [20] of:

$$\xi_g = \frac{\pi V_c \cos\theta_B}{\lambda F_g} \quad \text{Eq. (4)}$$

where V_c represents the volume of the α-Al unit cell, θ_B and F_g stand for the Bragg angle and structure factor for reflection $g(200)_{Al}$, respectively. The F_g value is equal to $4 \cdot f_\alpha$ for this reflection. f_α, which is the electron atomic scattering factor of the f.c.c. α-Al, can be calculated from the equation and parameters provided in the work of Peng [37] by considering the effect of high-energy accelerated electrons with a relativistic speed of v [38]. The equation for calculating f_α is as follows:

$$f_\alpha = [\sum_{i=1}^{n} a_i \cdot \exp(-b_i \frac{\sin^2\theta}{\lambda^2})] \cdot \left(\frac{1}{\sqrt{1-\frac{v^2}{c^2}}} \right) \quad \text{Eq. (5).}$$

The obtained theoretical value for ξ_g is 84.3 nm. This confirms that the selection of the *i* value and the calculation of *t* are correct.

The measured *t* value is then used to calculate the number density of Q precipitates growing along $[001]_{Al}$ in Fig. 2b. However, it is possible that in Fig. 2b some incomplete precipitates are cut by the surfaces of the TEM foil and thus have smaller lengths in the specimen region than the complete ones. While not all observed precipitates along $[001]_{Al}$ in Fig. 2b are completely contained in the foil, it is also possible that not all the incomplete precipitates contained can be distinguished. The BF image contrast for precipitates along $[001]_{Al}$ can be influenced by imperfections such as thickness fringes, bending contours and probably an uneven amorphous layer and contaminants on the foil surface, which give rise to non-uniform noise in the BF image. On the other hand, the interference by contrast from side-on precipitates along $[100]_{Al}$ and $[010]_{Al}$ is revealed in Fig. 2b. When the lengths of these incomplete precipitates are below a critical value of l_c, their contrast in the BF image will be very weak and can hardly be distinguished from the noise and the interference. Thus, the true number N_t of needle-like precipitates contained in this region should be larger than the N_v value measured from visible ones and should be adjusted. Precipitates are believed to be randomly distributed along the electron beam direction, as typically shown in Fig. 3a and conceptually simplified in Fig. 3b. The relationship between N_v and N_t is thus given as

$$N_v = N_t \cdot (l + t - 2 \cdot l_c) / (l + t) = 282 \quad \text{Eq. (6).}$$

Here a conservative assumption of

$$l_c = 0.1 \cdot t = 30.9 \text{ nm} \quad \text{Eq. (7)}$$

has been made, a verification of this choice will be provided in Section 3.3. Hence the N_t value is calculated as 332, and the weighted length of the precipitates (including complete and incomplete ones) growing along the electron beam direction has been calculated as

$$l_w = l \cdot (t - l) / (t + l) + l/2 \cdot 2 \cdot l/(t + l) = 77.2 \text{ nm} \quad \text{Eq. (8).}$$

The volume of the Q precipitates along $[001]_{Al}$ in the region shown in Fig. 2b can be therefore calculated as:

$$V_p^{[100]} = N_t \cdot l_w \cdot A_{cs} = 332 \times 77.2 \times 18.9 = 484415 \text{ nm}^3 \quad \text{Eq. (9),}$$

and the volume of the region is:

$$V_T = t \cdot A_{FOV} = 309.1 \times 661 \times 661 = 135052281 \text{ nm}^3 \quad \text{Eq. (10)}$$

where A_{FOV} denotes the area of the field of view in Fig. 2b. The volume fraction of the Q precipitates along $[001]_{Al}$ is $V_p^{[100]}/V_T$ = 0.359%. The total volume fraction of all the Q precipitates along $[100]_{Al}$, $[010]_{Al}$ and $[001]_{Al}$ can be calculated as 3 × 0.359% = 1.08%. The corresponding number density is then obtained as:

$$n = \frac{V_f}{l \cdot A_{cs}} = 5.41 \times 10^{21} \text{ m}^{-3} \quad \text{Eq. (11).}$$

3.2 Quantification of fine β"/C precipitates in the peak-aged microstructure

Similarly the volume fractions of the β" (including its less-developed precursor pre-β") and C precipitates in the peak-aged microstructure (aged for 8 h) have been measured as 1.11 % and 0.237 %, respectively, yielding a total volume fraction of 1.35 % for all the precipitates. The corresponding number densities are 2.15×10^{23} m^{-3} (for β" precipitates), 0.513×10^{23} m^{-3} (for C precipitates) or 2.67×10^{23} m^{-3} in total. The key images regarding the measurement are shown in Fig. 4.

The proportion of the number of each type of identified precipitate among all precipitates and the average area of the transverse cross-section of each type of precipitate are measured by HRTEM to derive the ratio between the volume fractions of β" and C. The average lengths of β" and C are assumed to be identical since (a) different side-on precipitates look similar in BF or HRTEM images and (b) the length-counts chart measured from Fig. 4a has only one distinguishable peak (see Section 3.5 for more details).

One difficult issue is that these precipitates are finer, both in length and diameter, than those in the sample aged for 30 d, thus the contrast from precipitates in BF images becomes weaker. As a result, thinner regions should be used to increase the contrast of the precipitates and thus to measure the average length and number (see Figs. 4a and 4b, respectively) of the precipitates. Careful comparison of BF and DF images (the latter shown in Fig. 4b, containing no influence from thickness fringes and bending contours) has been conducted to measure the number of precipitates parallel to the electron beam direction. The corresponding CBED pattern contains only two pairs of dark fringes in the $(200)_{Al}$

dark disk (see Fig. 4c), providing only two data points for calculating the *a* and *b* terms of Eq. (2). Such a calculation is certainly not reliable. To improve the reliability, a pair of bright fringes are introduced into the calculation, assigned with the n_k value of $i + 0.5$, according to the proposition of Allen [39]. The validity of the above proposition has been confirmed using the case of Q precipitates in a thicker region from which a similar straight line to that in Fig. 2d has been obtained. In this way an *i* value of 1 is found to produce a reasonable fitting of the line in Fig. 4d as well as the theoretical ξ_g value, thus the thickness of the region shown in Fig. 4b has been calculated as 68 nm and the above mentioned volume fractions have been obtained. A similar conservative assumption to Eq. (7) has been used here.

3.3 Verification of reliability of the CBED method by 3DAP

In order to verify the reliability of the method established for measuring the volume fraction of nano-precipitates in this work, especially the proposed Eq. (7), 3DAP has been applied to obtain the number density of β"/C precipitates in the sample aged for 8 h, as shown in Fig. 5. Since these precipitates are densely distributed within a volume of ~130×60×60 nm^3, the reliability of the statistics can be guaranteed. In this work, a precipitate number density of 3.85 $\times 10^{23}$ m^{-3} with an estimated standard deviation of $\pm$ 0.33$\times 10^{23}$ m^{-3} has been obtained. This value can be regarded as important verification for the number density measured by the CBED method in spite of possible error.

However, making a direct comparison between the number densities obtained from the CBED method and 3DAP analysis is impossible. In the former the influence of incomplete precipitates was compensated for and the obtained value represents an infinite volume, while both complete and incomplete precipitates were included as such in the latter. The 3DAP specimen volume is approximately equal to a truncated cone with a top diameter of 50.6 nm (see D_1 in Fig. 5b), bottom diameter of 66.4 nm (D_2) and a height of 134.5 nm (H). The nearly same shape of the specimen under different rotations along its long axis, as shown in Figs. 5a and 5c, confirms this geometry. The size of the specimen implies there is a large fraction of incomplete precipitates as schematically shown in Fig. 5b. In order to compare the two number densities expressed in different forms, one has to first estimate how many complete and incomplete precipitates should exist in the 3DAP specimen volume according to the number density obtained from the CBED method. Therefore a simplified 3D model has been established (see Fig. 5b) by considering the 3DAP specimen volume (marked by solid lines),

orientations of precipitates (represented by angle α) and the average length of precipitates. In this model, all precipitates are simplified to have the same length, i.e. the measured average length l. A precipitate with its center located within the two truncated cones marked by dashed lines in Fig. 5b is incomplete within the specimen volume. The geometrical parameters of the two dashed truncated cones, including D_1', D_2', H', D_1'', D_2'' and H″ were calculated from the parameters D_1, D_2, H, α and l. The number of all nano-precipitates belonging to the same growth direction (i.e., with the same α value), regardless their nature of being complete or incomplete within the solid truncated cone, can be estimated from the number density measured in the CBED method by artificially shrinking them into point objects within the outer dashed truncated cone. The correspondingly estimated number density containing all growth directions is 3.68×10^{23} m^{-3}. The value is close to the one of 3.85×10^{23} m^{-3} directly measured by 3DAP, the low mismatch of 4.5% confirming the assumption of $l_c = 0.1\cdot t$ used in Sections 3.1-3.2 as being reasonable.

In the future, a more reliable estimation of the l_c value from simulations of contrast between the precipitate and α-Al matrix by considering factors such as crystal structures and multiple scattering could be obtained for further improving the accuracy of determination of precipitate number density.

3.4 Estimation for the error of the measurements

The equation for calculating precipitate volume fraction has been summarized and transformed to the following form, which contains only directly measured values:

$$V_f = \frac{3\cdot N_t \cdot l_w \cdot A_{cs}}{t\cdot a^2} = \frac{3\cdot N_v \cdot l \cdot A_{cs}}{(l+0.8t)\cdot a^2} \qquad \text{Eq. } (12)$$

The precision of the V_f value obtained can be estimated from the equation for propagation of uncertainty [40]. According to the measuring processes and origin of uncertainties during the measurements, uncertainties in the form of standard deviation S_{Nv}, S_l, S_{Acs}, S_t and S_a are estimated to be ±10%, ±6%, ±10%, ±3% (according to the evaluation in [22]) and ±2% (according to scale bar calibration of HRTEM images) of the measured values, respectively. The reason for assigning N_v a relative uncertainty of 10% is that the ratio of 0.1 in Eq. (7) was roughly estimated, although they were later verified by 3DAP in Section 3.3. The reason for assigning A_{cs} a relative uncertainty of 10% is that the precipitate/matrix interface is usually not straight and is thus hard to locate, meanwhile the average

precipitate cross-section area was measured from only about 20 precipitates. With these inputs, the uncertainties of the Q and β"/C volume fractions are calculated as ±0.17 vol.% and ±0.21 vol.%, yielding relative uncertainties of ±16 % in both cases. In contrast, the S_t/t value of the EELS method is greater than ±8% for aluminum and the produced S_{Vf}/V_f value can be increased by about 1%.

The precision of the number density measured, which is expressed in the equation of:

$$n = \frac{V_f}{l \cdot A_{cs}} = \frac{3 \cdot N_v}{(l + 0.8t) \cdot a^2} \qquad \text{Eq. } (13)$$

can be estimated in a similar way. The calculated relative uncertainty of the two measurements in this work is ±11% for both cases. The data measured in this work has been summarized in Tab. 1.

3.5 Computational method for estimating number density and volume fraction from measured parameters

To reach the highest reliability for calculating number density and volume fraction of precipitates with the parameters measured, a computational method containing the following steps has been applied:

(1) Analyze the distributions of lengths and cross-section areas of precipitates. The length distribution was found to match the inverse Gaussian distribution well, as shown in Fig. 6. The cross-section areas of precipitates were not fitted since only about 20 precipitates were measured in each alloy sample.

(2) The fitted distributions were then used to generate random values for precipitate length l, uniform distributions were used to generate spatial coordinates (x, y, z) of the precipitate core. The z direction was defined as the thickness direction and the foil sample was treated with $z \in (-t/2, t/2)$. If the parameters of a precipitate follow the inequality of

$$|z| < t/2 - l_c + l/2 = 0.4\ t + l/2 \qquad \text{Ineq. } (1),$$

then this precipitate is believed to be visible according to Eq. *(7)*. 282 such precipitates were generated in total for sample 1# as shown in Fig. 7a.

(3) For each precipitate, if $|z| < 0.4\ t - l/2$, then it is a complete precipitate in the sample volume with $z \in (-0.4t, 0.4t)$ and one can set i=1; if $0.4\ t - l/2 < |z|$, then the precipitate is incomplete and one can set $i = (0.4\ t + l/2 - |z|)/l$. The number density of precipitates should be calculated as

$$n = 3 \cdot \sum_{N=1}^{282} i_N / (A_{FOV} \cdot 0.8t) \quad \text{Eq. (14)}$$

for the case of sample 1# shown in Fig. 2b. The corresponding volume fraction can then be calculated as:

$$V_f = 3 \cdot \sum_{N=1}^{282} i_N \cdot l_N \cdot A_{cs} / (A_{FOV} \cdot 0.8t) \quad \text{Eq. (15).}$$

As there were random values generated in step (2), steps (2-3) were performed 10,000 times and results were averaged to increase the reliability. The final n and V_f values for Q precipitates are 5.58×10^{21} m^{-3} and 1.05%, respectively. Similarly, the n and V_f values for β"/C precipitates in sample 2# were calculated as 2.67×10^{23} m^{-3} and 1.35% (see Tab. 1). These data are in good agreement with the data obtained by the CBED based on calculations in Sections 3.1-3.2, reflecting that the use of a mean precipitate length in those calculations does not result in a considerable additional error. The Matlab code for computing number density and volume fraction of precipitates in sample 1# has been included in the Appendix.

3.6 Procedures, limitations and advantages of the CBED method established

The method of measuring precipitate volume fraction based on CBED, as established in this work, can be summarized into the following procedures:

(1) Length: observe the thin foil sample along $[001]_{Al}$ in low-magnification TEM images to measure the average length of side-on needle-like nano-precipitates, preferably in a moderately thin region to maximize the precipitate contrast. The larger the statistic the more reliable the measurement.

(2) Cross-section area: measure the average cross-section area of end-on precipitates by HRTEM in the same thin region. A large statistic is of course preferred but requires a long time.

(3) Number counting: find a moderately thick region but meanwhile make sure the end-on precipitates are clearly visible. Count the number of end-on precipitates.

(4) Sample thickness: tilt the $[001]_{Al}$ zone axis slightly away from the electron beam direction by about 4-5º to reach the two-beam condition, record the CBED pattern and the two groups of (α, β) angles before and after tilting. Calculate the untilted foil thickness based on the pattern

and Eqs. (1-5).

(5) Number density and volume fraction: calculate the number density and volume fraction of nano-precipitates according to the values obtained in steps (1-4) and Eqs. (6-11). Or one can use the computational method given in Section 3.5 and the Appendix.

It is worth noting that this method has at least the following 4 limitations:

(1) *Crystal*: the matrix should be crystalline, otherwise it is impossible to measure foil thickness by CBED.

(2) *Foil thickness*: in practice, the TEM foil thickness (across the electron beam direction) at the two-beam condition should not be smaller than ~80% of ξ_g, the extinction distance of the reflection targeted, according to the example in Fig. 4. More details concerning the calculation of the measurable thickness range, which varies with instrument voltage and reflection, can be found in the work of Allen [39]. The situation in Fig. 4c is almost reaching this critical condition. With a smaller foil thickness, the second bright fringe in the dark disk will move out of the disk and could not be located. This also limits the smallest size of precipitates observable in the region.

(3) *Well defined geometry*: the precipitate should have a well-defined shape so that its average volume can be precisely measured.

(4) *Precipitate size*: the precipitate size should be close to or larger than 10 nm in at least one dimension, so that it can be clearly observed in low-magnification TEM images. On the other hand, most of the precipitates should be complete within the specimen volume. Preferentially, the largest dimension of the precipitate should be smaller than half the specimen thickness. Generally, a precipitate size of about 10 to 200 nm is suitable for the CBED method used in this work.

Working within these limitations, the method has apparent advantages as listed below:

(1) *Superb accessibility*: it can be performed on any modern LaB_6 [41] or FEG high-resolution transmission electron microscope alone without any additional instrument or special apparatus, since using these instruments to resolve the transverse cross sections of the nano-precipitates in HRTEM imaging mode is not difficult.

(2) *Convenience*: the method does not demand any special specimen like the needle specimen for quantitative electron tomography [13].

(3) *Moderate efficiency*: 2 hours on microscope is enough for collecting the images required, the data interpretation needs only another 2 hours or less.

(4) *Acceptable accuracy and precision*: the precision of the determined volume fraction is around ±16% while that of the number density is about ±11%, the latter has been verified by 3DAP.

4. Conclusions

A facile method based on the CBED technique has been established to measure the volume fraction of nano-precipitates in crystalline materials with acceptable accuracy and precision, using the case studies of needle-like β″/C and Q precipitates in an aged Al-Mg-Si-Cu alloy as well as verifications by 3DAP analysis. The detailed characteristics of the method are:

(1) The thickness of the TEM thin foil can be accurately calculated from a CBED pattern taken in two-beam condition, with a low uncertainty of ±3%. The number density and volume fraction of the precipitates in the observed region can then be calculated with the number and size of precipitates measured in low-magnification and HRTEM images. In the present case, the uncertainties for these two quantities are 11% and 16%, respectively, which is an improvement over the existing approaches.

(2) The generally believed thickness detection limit of $t > \xi_g$ (extinction distance) can be practically extended to $t > 0.8 \cdot \xi_g$, by considering both the bright and dark fringes in the dark disk of a CBED pattern.

(3) The effect of indistinguishable contrast of the too short incomplete precipitates ($l < l_c$) cut by the foil surfaces, was taken into account and compensated for by an equation of $l_c = 0.1 \cdot t$, in order to increase the accuracy of the method. The reasonability of this equation has been confirmed since the number density obtained in this way is comparable to the one directly measured by 3DAP with a low mismatch of 4.5%.

(4) The method can be efficiently performed on a regular TEM foil specimen with any modern transmission electron microscope, and it is highly dependable for measurement of volume fraction of fine nano-precipitates in a well-defined shape, of which the largest dimension varies from about 10 to 200 nm.

Acknowledgement

This work is financially supported by National Natural Science Foundation of China (51501230 and 51531009) and Postdoctoral Science Foundation of Central South University (502042057). H.I.

acknowledges the IAP program of the Belgian State Federal Office for Scientific, Technical and Cultural Affairs under Contract No. P7/21 and FWO project G.0576.09N.

References

[1] Q. Du, W.J. Poole, M.A. Wells, A mathematical model coupled to CALPHAD to predict precipitation kinetics for multicomponent aluminum alloys, Acta Mater., 60 (2012) 3830-3839.

[2] G.B. Olson, C.J. Kuehmann, Materials genomics: From CALPHAD to flight, Scripta Mater., 70 (2014) 25-30.

[3] B. Böttger, J. Eiken, I. Steinbach, Phase field simulation of equiaxed solidification in technical alloys, Acta Mater., 54 (2006) 2697-2704.

[4] V. Fallah, A. Korinek, N. Ofori-Opoku, N. Provatas, S. Esmaeili, Atomistic investigation of clustering phenomenon in the Al–Cu system: Three-dimensional phase-field crystal simulation and HRTEM/HRSTEM characterization, Acta Mater., 61 (2013) 6372-6386.

[5] S. Esmaeili, D.J. Lloyd, W.J. Poole, A yield strength model for the Al-Mg-Si-Cu alloy AA6111, Acta Mater., 51 (2003) 2243-2257.

[6] C.D. Marioara, S.J. Andersen, H.W. Zandbergen, R. HOLMESTAD, The influence of alloy composition on precipitates of the Al-Mg-Si system, Metall. Mater. Trans. A, 36A (2005) 691-702.

[7] W.F. Miao, D.E. Laughlin, Effects of Cu content and preaging on precipitation characteristics in aluminum alloy 6022, Metall. Mater. Trans. A, 31A (2000) 361-371.

[8] P.J. Withers, X-ray nanotomography, Materials Today, 10 (2007) 26-34.

[9] B.R. Pinzer, A. Medebach, H.J. Limbach, C. Dubois, M. Stampanoni, M. Schneebeli, 3D-characterization of three-phase systems using X-ray tomography: tracking the microstructural evolution in ice cream, Soft Matter, 8 (2012) 4584.

[10] M.D. Uchic, M.A. Groeber, D.M. Dimiduk, J.P. Simmons, 3D microstructural characterization of nickel superalloys via serial-sectioning using a dual beam FIB-SEM, Scripta Mater., 55 (2006) 23-28.

[11] S. Cao, S. Pourbabak, D. Schryvers, Quantitative 3-D morphologic and distributional study of Ni4Ti3 precipitates in a Ni51Ti49 single crystal alloy, Scripta Mater., 66 (2012) 650-653.

[12] S. Bals, G. Van Tendeloo, C. Kisielowski, A New Approach for Electron Tomography: Annular Dark-Field Transmission Electron Microscopy, Adv. Mater., 18 (2006) 892-895.

[13] G. Van Tendeloo, S. Bals, S. Van Aert, J. Verbeeck, D. Van Dyck, Advanced electron microscopy for advanced materials, Adv. Mater., 24 (2012) 5655-5675.

[14] L. Molina, H. Tan, E. Biermans, K.J. Batenburg, J. Verbeeck, S. Bals, G.V. Tendeloo, Barrier efficiency of sponge-like La2Zr2O7 buffer layers for YBCO-coated conductors, Supercond. Sci. Technol., 24 (2011) 065019.

[15] C.D. Marioara, H. Nordmark, S.J. Andersen, R. Holmestad, Post-β″ phases and their influence on microstructure and hardness in 6xxx Al-Mg-Si alloys, J. Mater. Sci., 41 (2006) 471-478.

[16] C.D. Marioara, S.J. Andersen, T.N. Stene, H. Hasting, J. Walmsley, A.T.J. Van Helvoort, R. Holmestad, The effect of Cu on precipitation in Al–Mg–Si alloys, Philos. Mag., 87 (2007) 3385-3413.

[17] S. Esmaeili, X. Wang, D.J. Lloyd, W.J. Poole, On the precipitation-hardening behavior of the Al-Mg-Si-Cu alloy AA6111, Metall. Mater. Trans. A, 34A (2003) 751-763.

[18] C.S. Tsao, U.S. Jeng, C.Y. Chen, T.Y. Kuo, Small-angle X-ray scattering study of

nanostructure evolution of β″ precipitates in Al–Mg–Si alloy, Scripta Mater., 53 (2005) 1241-1245.

[19] C.S. Tsao, C.Y. Chen, U.S. Jeng, T.Y. Kuo, Precipitation kinetics and transformation of metastable phases in Al–Mg–Si alloys, Acta Mater., 54 (2006) 4621-4631.

[20] D.B. Williams, C.B. Carter, *Transmission electron microscopy: a textbook for materials science*, Springer Science+Business Media, New York, 2009.

[21] A. Bardal, K. Lie, Measuring the thickness of aluminium alloy thin foils using electron energy loss spectroscopy, Mater. Charact., 44 (2000) 329-343.

[22] S.M. Allen, E.L. Hall, Foil thickness measurements from convergent-beam diffraction patterns An experimental assessment of errors, Philos. Mag. A, 46 (1982) 243-253.

[23] Y. Berta, C. Ma, Z.L. Wang, Measuring the aspect ratios of ZnO nanobelts, Micron, 33 (2002) 687-691.

[24] G. Sha, H. Möller, W.E. Stumpf, J.H. Xia, G. Govender, S.P. Ringer, Solute nanostructures and their strengthening effects in Al–7Si–0.6Mg alloy F357, Acta Mater., 60 (2012) 692-701.

[25] D. Vaumousse, A. Cerezo, P.J. Warren, A procedure for quantification of precipitate microstructures from three-dimensional atom probe data, Ultramicroscopy, 95 (2003) 215-221.

[26] K. Li, A. Béché, M. Song, G. Sha, X. Lu, K. Zhang, Y. Du, S.P. Ringer, D. Schryvers, Atomistic structure of Cu-containing β″ precipitates in an Al–Mg–Si–Cu alloy, Scripta Mater., 75 (2014) 86-89.

[27] K. Li, M. Song, Y. Du, Y. Tang, H. Dong, S. Ni, Investigation of the as-solidified microstructure of an Al–Mg–Si–Cu alloy, J. Alloy Compd., 602 (2014) 312-321.

[28] M.K. Miller, Atom Probe Tomography: Analysis at the Atomic Level, Kluwer Academic/Plenum, New York, 2000.

[29] M.K. Miller, A. Cererzo, M.G. Hetherington, G.D.W. Smith, Atom Probe Field Ion Microscopy, Oxford University Press Inc, New York, 2006.

[30] G. Sha, Y.B. Wang, X.Z. Liao, Z.C. Duan, S.P. Ringer, T.G. Langdon, Influence of equal-channel angular pressing on precipitation in an Al–Zn–Mg–Cu alloy, Acta Mater., 57 (2009) 3123-3132.

[31] J. Buha, R.N. Lumley, A.G. Crosky, K. Hono, Secondary precipitation in an Al–Mg–Si–Cu alloy, Acta Mater., 55 (2007) 3015-3024.

[32] M. Torsæter, F.J.H. Ehlers, C.D. Marioara, S.J. Andersen, R. Holmestad, Applying precipitate–host lattice coherency for compositional determination of precipitates in Al–Mg–Si–Cu alloys, Philos. Mag., 92 (2012) 3833-3856.

[33] S.J. Andersen, H.W. Zandbergen, J. Jansen, C. TrÆholt, U. Tundal, O. Reiso, The crystal structure of the β″ phase in Al–Mg–Si alloys, Acta Mater., 46 (1998) 3283-3298.

[34] H.W. Zandbergen, Structure Determination of Mg5Si6 Particles in Al by Dynamic Electron Diffraction Studies, Science, 277 (1997) 1221-1225.

[35] K. Li, M. Song, Y. Du, H. Zhang, Simulation of the electron diffraction patterns from needle/rod-like precipitates in Al–Mg–Si alloys, Mater. Charact., 62 (2011) 894-903.

[36] M. Fiawoo, X. Gao, L. Bourgeois, N. Parson, X.Q. Zhang, M. Couper, J.F. Nie, Formation of multiple orientation relationships of Q precipitates in Al–Mg–Si–Cu alloys, Scripta Mater., 88 (2014) 53-56.

[37] L.M. Peng, Electron atomic scattering factors and scattering potentials of crystals, Micron, 30 (1999) 625-648.

[38] P.A. Doyle, Relativistic Hartree-Fock X-ray and electron scattering factors, Acta

Crystallographica Section A, 24 (1968) 390-397.

[39] S.M. Allen, Foil thickness measurements from convergent-beam diffraction patterns, Philos. Mag. A, 43 (1981) 325-335.

[40] URL://en.wikipedia.org/wiki/Propagation_of_uncertainty.

[41] D. Schryvers, Order-disorder phenomena in the binary alloys PtxTi, PtxV ($3 \leq x \leq 8$) and Ni3Mo studied by high resolution electron microscopy, Ph. D in Physics, University of Antwerp, 1985

Figure captions

Figure 1. Two examples are shown of measuring the thickness by counting the extinction fringes in TEM images. The images were taken from: (a) the edge of a hole and (b) an inclined grain boundary (GB) in an aged Al-Mg-Si-Cu sample containing nano-precipitates. The orders of the fringes are indexed in the images, among which the value of i is not known. The zone axis of (a) and the lower grain in (b) is $[001]_{Al}$.

Figure 2. The measuring process of key parameters for calculating the volume fraction of Q nano-precipitates in the sample aged for 30 d. The average precipitate length (see red solid rectangles) was measured from a series of TEM BF image taken along $[001]_{Al}$ such as (a), and the average area of the transverse cross-section was measured from the HRTEM images shown as insets. Incomplete particles extending outside the field of view (see the blue dashed rectangle) are not included in the measurement. The number of needle-like precipitates along $[001]_{Al}$ is counted from another BF image in (b) along $[001]_{Al}$, α tilt of the specimen is -15.94˚, β tilt is -3.57˚. A CBED pattern shown in (c) is then taken via a slight tilt from the $[001]_{Al}$ direction of the same region. α tilt of the specimen is -14.79˚, β tilt is 1.26˚. The intensity line profile from A-B is shown in the lower part. The relationship between S_i^2/n_k^2 and $1/n_k^2$ is linearly fitted with $i = 4$ as shown in (d).

Figure 3. Schematic description of the relationship between the true number N_t and visible number N_v of the needle-like precipitates growing along the zone axis of $[001]_{Al}$. N_t precipitates along $[001]_{Al}$ are contained in an observed volume of the foil specimen, but only N_v of them are visible since in TEM a needle shorter than l_c would present very weak contrast. In the left part the precipitates are randomly distributed, in the right part the precipitates are manually shifted for simplification.

Figure 4. The measurement of the parameters needed for calculating the volume fraction of needle-like β″/C nano-precipitates in the sample aged for 8 h. The average length of the precipitates is measured in (a) a BF image of a thin region nearby the hole in the TEM thin foil, Z = $[001]_{Al}$. The length distribution of the precipitates is analyzed in the length-counts chart inserted, where the increment of length is 1.5 nm. The number of precipitates along $[001]_{Al}$ is counted in (b) a DF image (by selecting some reflections in the diffraction pattern in the

inset, Z = $[001]_{Al}$) from a moderately thin region nearby. The thickness of this region (68 nm) can be calculated from (c) the corresponding CBED pattern taken in the two-beam condition reached by a slight tilt. The calculation is done by linear fitting of the relationship between S_i^2/n_k^2 and $1/n_k^2$ with $i = 1$ in (d).

Figure 5. Comparison of the number densities of β″/C nano-precipitates measured by the CBED method and 3DAP in the sample aged for 8 h. (a) is the distribution of Mg within precipitates visualized by 3DAP analysis, the zone axis is close to $[001]_{Al}$, the specimen volume is simplified into a truncated cone in (b) and a 3D model has been constructed to estimate how many precipitates should exist within the 3DAP specimen volume according to the number density measured by the CBED method (see section 3.3 for more details). It should be noted that precipitates *i*-*v* are incomplete in the specimen volume. The number density of the precipitates is also directly measured by 3DAP as shown in (c).

Figure 6. Length distributions of (a) Q and (b) β″/C precipitates in samples 1# and 2#, respectively. The experimental distributions (see the bars) were fitted by Inverse Gaussian distribution (see the red curves) with the parameters provided in brackets.

Figure 7. Computed random distributions of the visible precipitates along $[001]_{Al}$ in (a) sample 1# and (b) sample 2#, corresponding to Fig. 2b and Fig. 4b, respectively. See Section 3.5 for details.

Table 1. Measured and estimated quantities by TEM and 3DAP. Data in brackets indicate standard error, *N* represents the (statistical) sample size, the symbols ± are followed by estimated error for the data before the symbols.

Sample	1#: aged for 30 d	2#: aged for 8 h
Nano-precipitate type	Q (Fig. 2)	β″/C (Fig. 4)
Length $\boldsymbol{l}$	103(3.7) nm (*N*= 292)	11.4(0.40) nm (*N*= 190)
Area of cross section $\boldsymbol{A_{cs}}$	18.9(1.9) nm^2 (*N*=17)	4.45(0.25) nm^2 (*N*=26)
Specimen thickness $\boldsymbol{t}$	309 nm	68 nm
Volume fraction $\boldsymbol{V_f}$ by CBED	1.08±0.17 %	1.35±0.21 %
$\boldsymbol{V_f}$ by the computational method	1.05% (*N*=10000)	1.35% (*N*=10000)
Number density $\boldsymbol{n}$ by CBED	$5.53\pm0.60\times10^{21}$ m^{-3}	$2.66\pm0.30\times10^{23}$ m^{-3}
$\boldsymbol{n}$ by the computational method	5.58×10^{21} m^{-3} (*N*=10000)	2.67×10^{23} m^{-3} (*N*=10000)
Estimated number density in 3DAP specimen volume from $\boldsymbol{n}$	/	3.68×10^{23} m^{-3}
Number density by 3DAP	/	$3.85 \pm 0.33\times10^{23}$ m^{-3}

Appendix

Matlab code for computing number density and volume fraction of precipitates in sample 1#.

```
%One should first measure the length distribution and analyze the data using the dfittool in Matlab.
%l= [l1,l2,l3.....];
%dfittool
%Here an Inverse Gaussian distribution with parameters of mu=102.929 and lambda=272.891 was found to best fit the raw experimental data.
%=============Run Here====================
n=1,
B=zeros(10000,2);

while n<=10000; %Run 10000 times, one could change the n value to reduce calculation time.
A=zeros(282,7); %There were 282 precipitates found growing along [001]Al in the field of view
i=1;
xi=unifrnd(0,661); %generate random x coordinate for a precipitate
yi=unifrnd(0,661); %generate random y coordinate for a precipitate
zi=unifrnd(-290,290); %generate random z coordinate for a precipitate
li=random('inversegaussian', 102.929, 272.891); %generate random length for a precipitate according to the Inverse Gaussian distribution
while i<=282
if (abs(zi)<123.6+li/2)&(li>0)&(li<320) %judge if this precipitate are visible in the foil sample or not, see Ineq. (1)
A(i,1)=xi;
A(i,2)=yi;
A(i,3)=zi;
A(i,4)=li;
A(i,5)=i;
i=i+1; %if yes, accept the precipitate
end
zi=unifrnd(-290,290);
xi=unifrnd(0,661);
yi=unifrnd(0,661);
li=random('inversegaussian', 102.929, 272.891); % if not, generate another precipitate
end

i=1;
while i<=282;
if abs(A(i,3))<123.6-A(i,4)/2
A(i,6)=1;
A(i,7)=A(i,6)*A(i,4)*18.8916;%volume of a complete precipitate,18.8916 is the area of precipitate cross section in nm^2
i=i+1;
else
A(i,6)=(123.6+A(i,4)/2-abs(A(i,3)))/A(i,4);
A(i,7)=A(i,6)*A(i,4)*18.8916; %volume of a incomplete precipitate
i=i+1;
end
end
B(n,1)=3*sum(A(:,6))/(661e-9*661e-9*309e-9*0.8); % Calculating nunber Density, area of field of view = 661*661nm2, thickness = 309 nm, this calculation considers precipitates contained in 80% of the thickness
B(n,2)=3*sum(A(:,7))*1e-27/(661e-9*661e-9*309e-9*0.8); %Volume Fraction
n=n+1;
```

```
1  n
2  end
3  %One has now 10000 groups of n & V_f values at hand, use the dfittool to get the average values and
4  standard deviations.
```

High-resolution Figure 1
Click here to download high resolution image

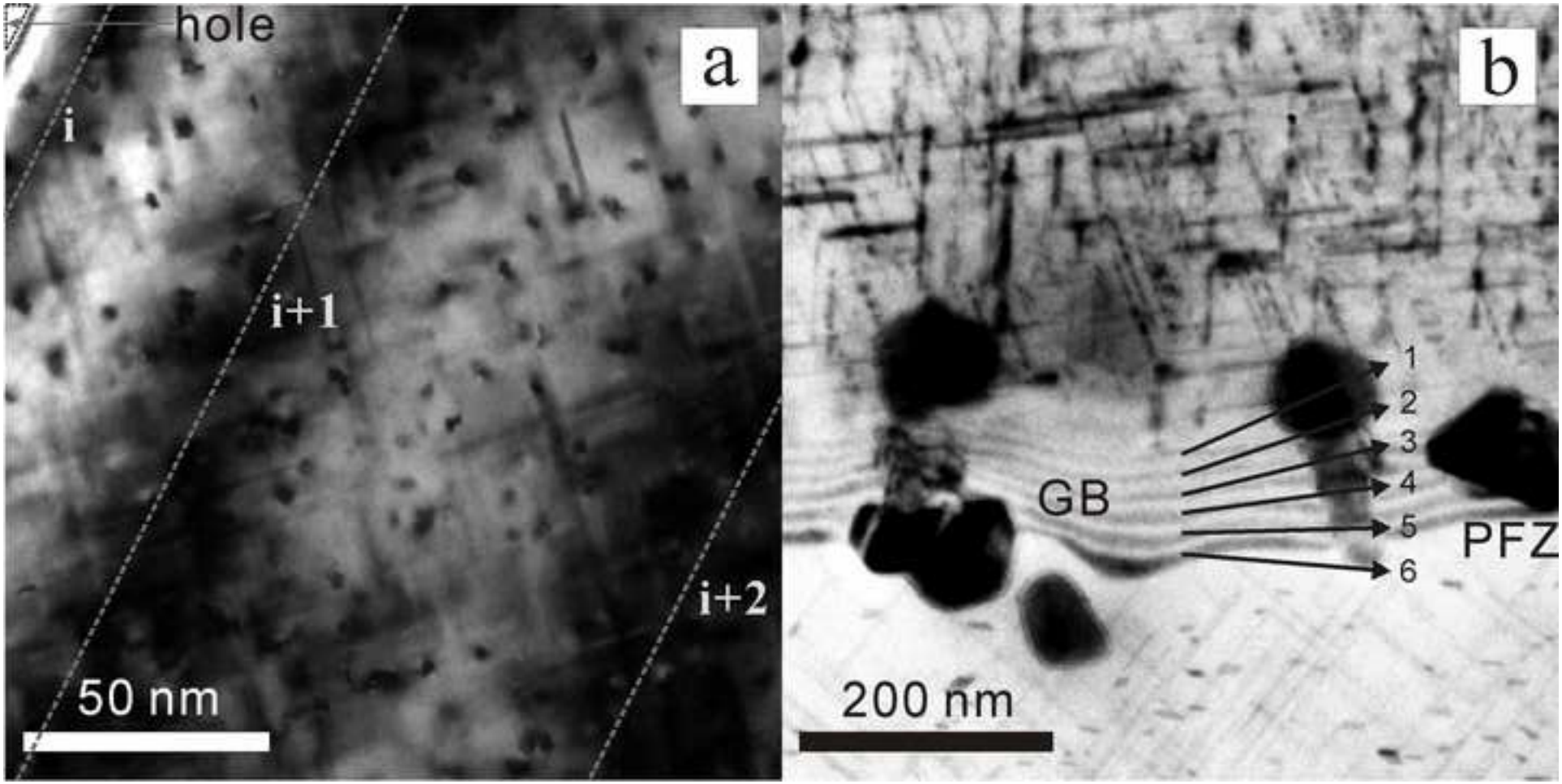

High-resolution Figure 2

Click here to download high resolution image

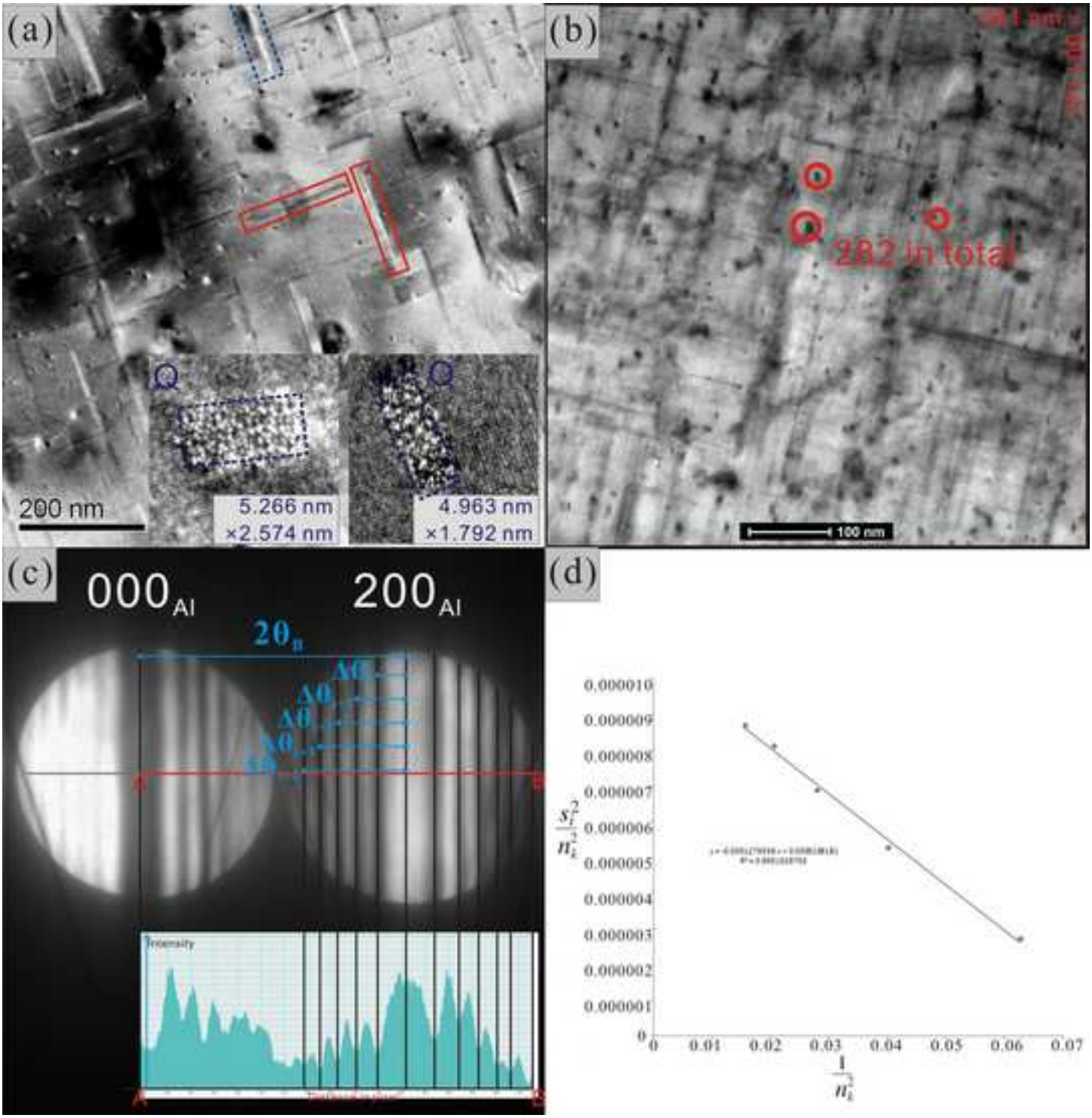

High-resolution Figure 3

Click here to download high resolution image

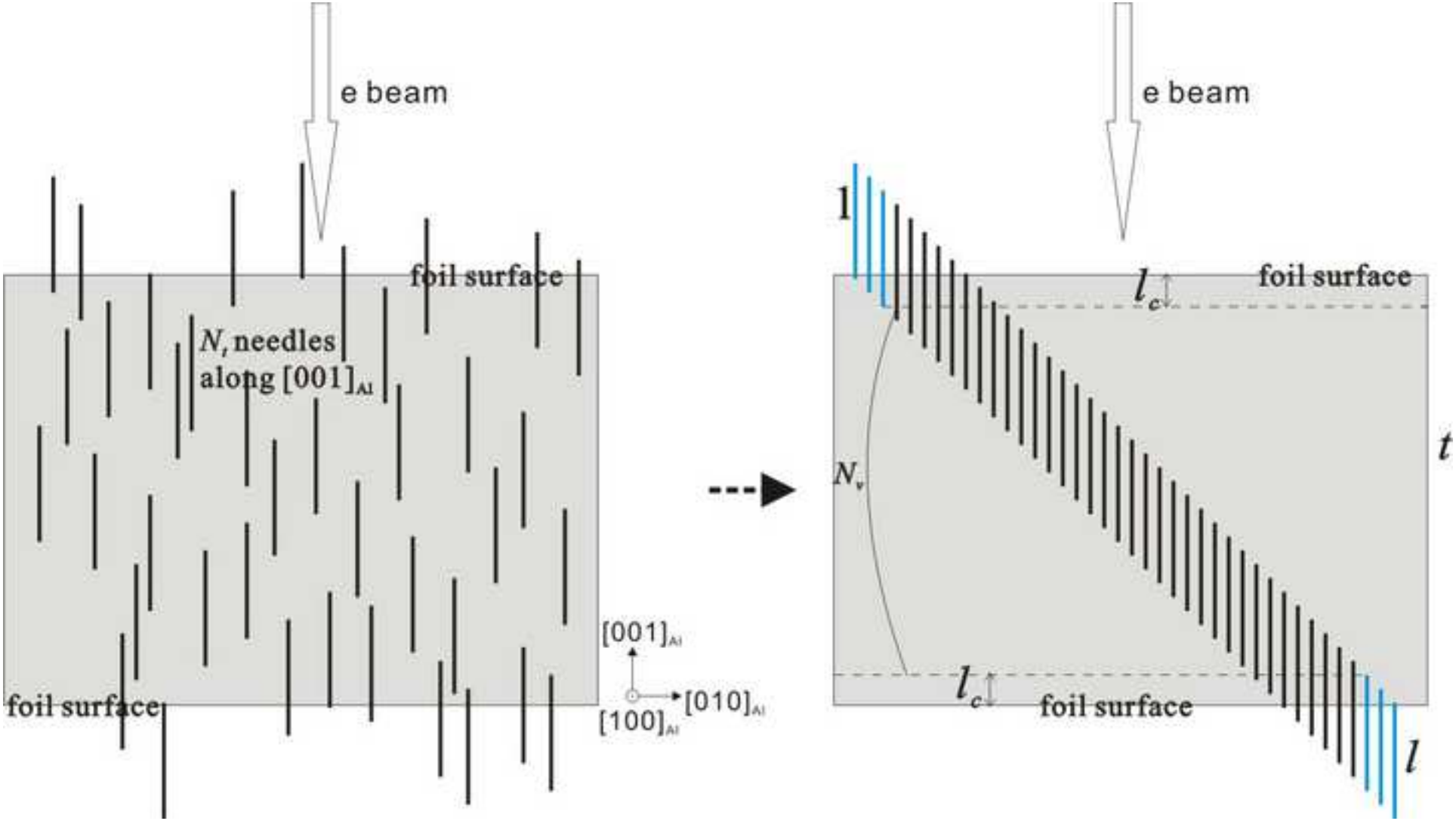

High-resolution Figure 4

Click here to download high resolution image

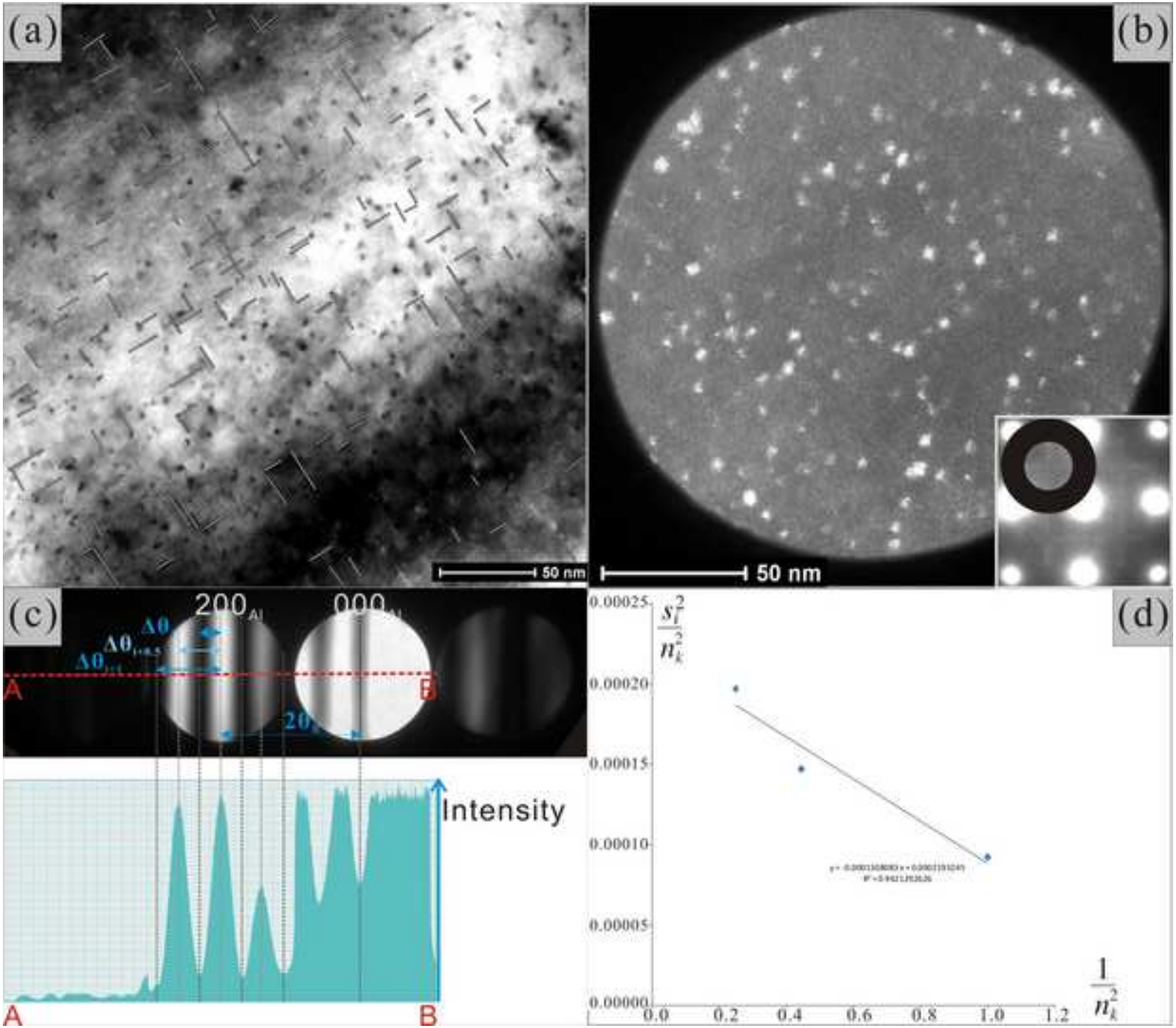

High-resolution Figure 5

Click here to download high resolution image

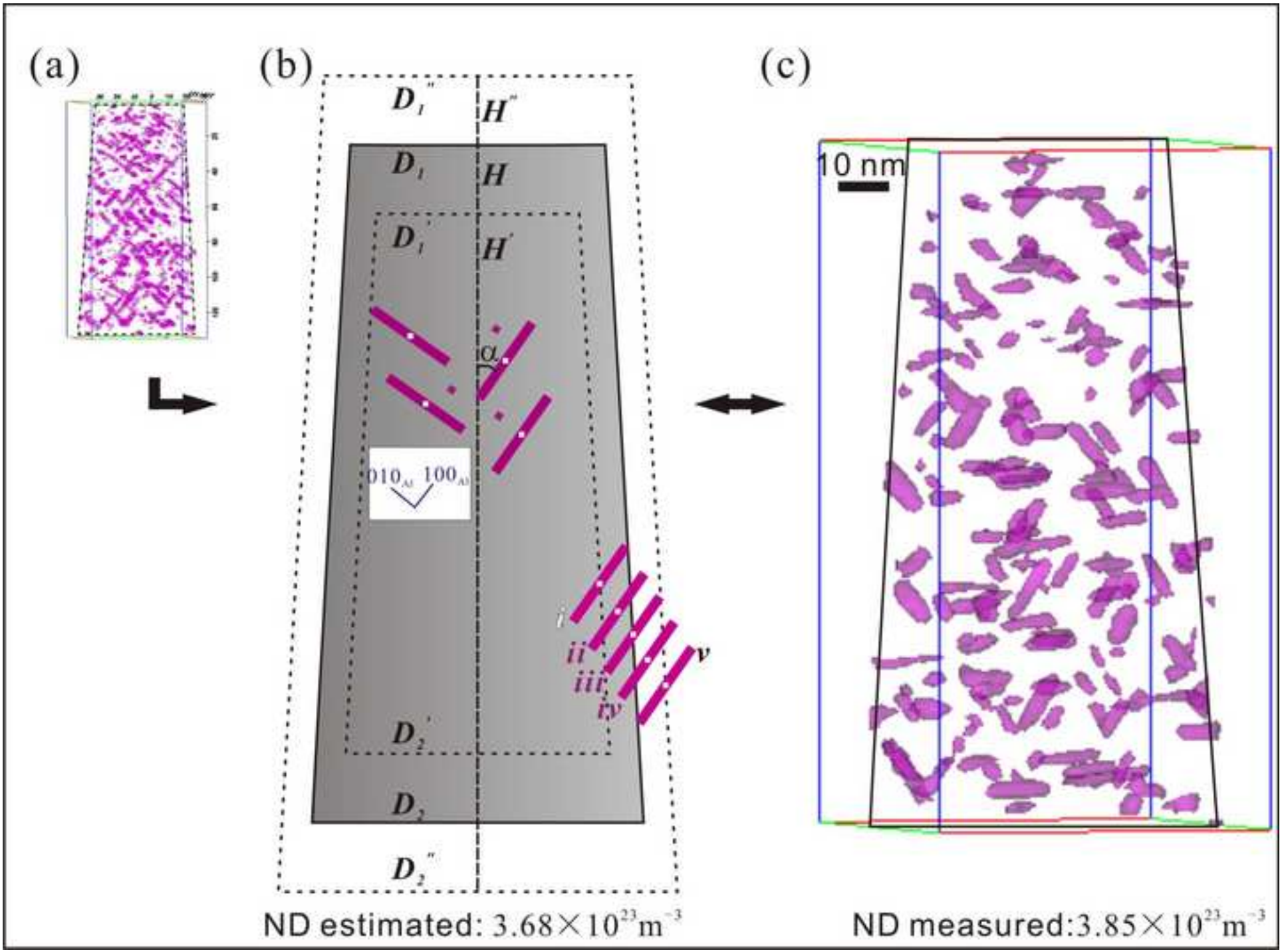

High-resolution Figure 6

Click here to download high resolution image

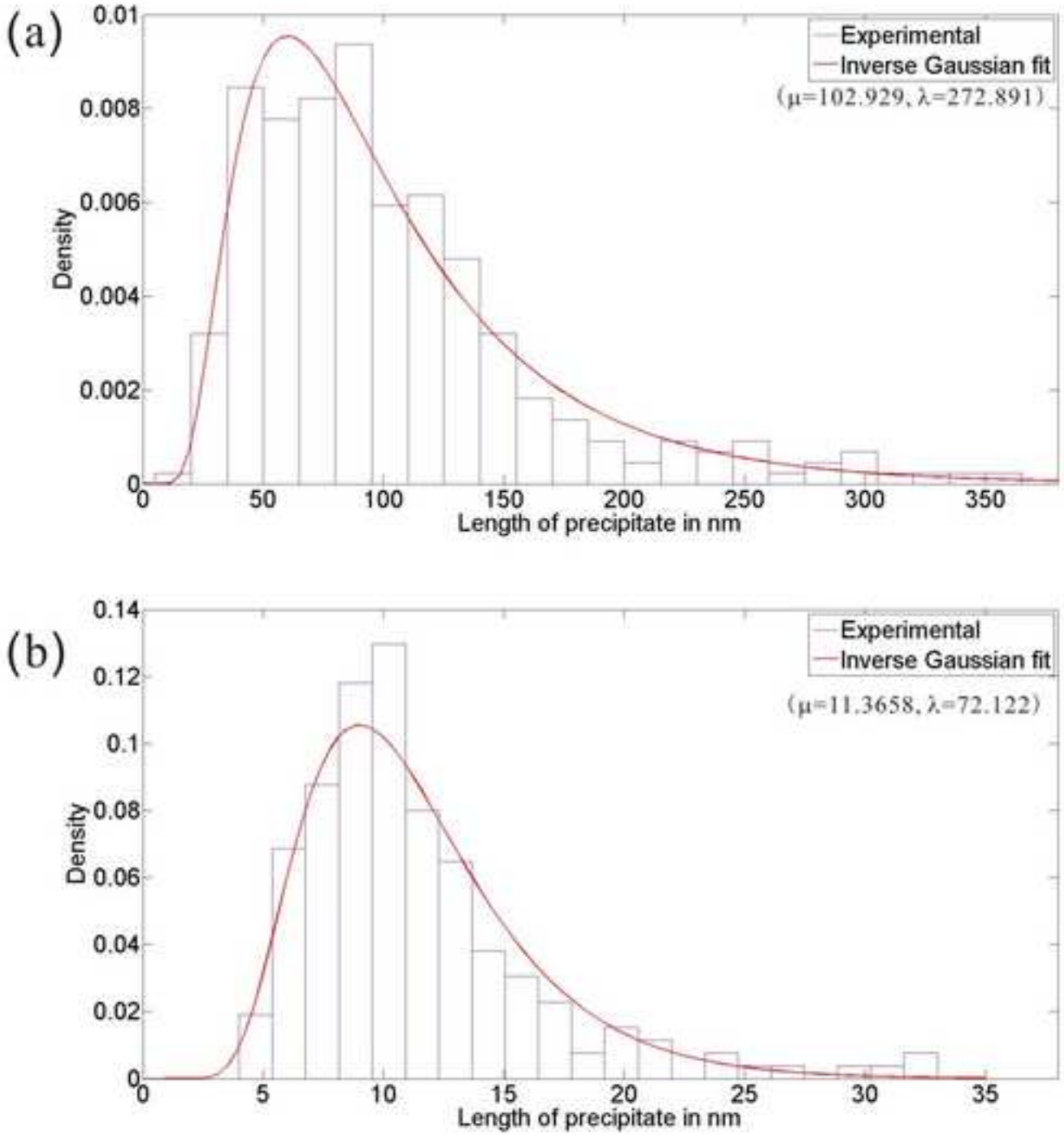

High-resolution Figure 7
Click here to download high resolution image

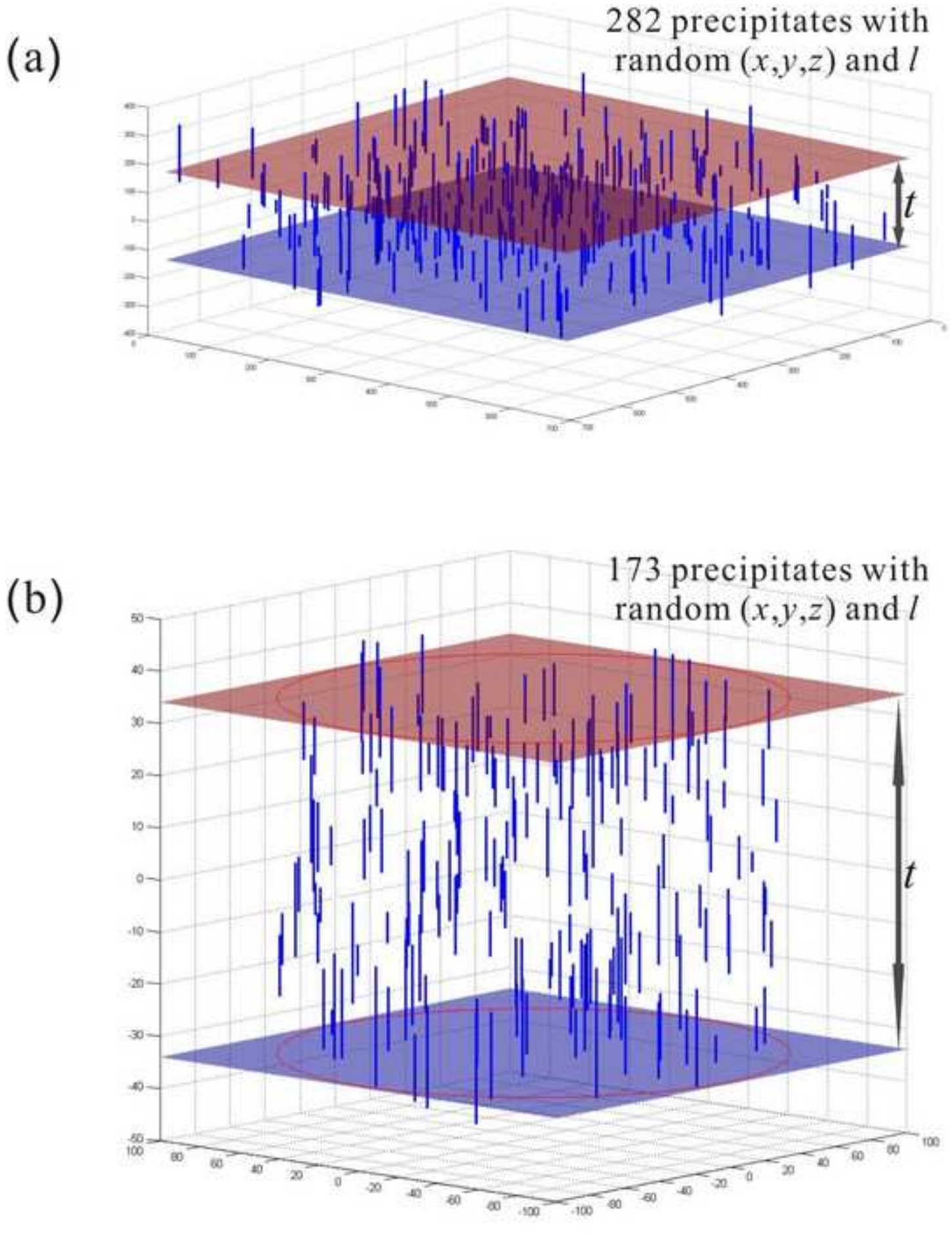

Supplementary Material

Click here to download Supplementary Material: Supplement-revised.docx